Optimal Trajectories for Aircraft Avoidance of Multiple Weapon Engagement Zones

Patrick M. Dillon* and Michael D. Zollars†
Air Force Institute of Technology, Wright-Patterson Air Force Base, Ohio, 45433

Isaac E. Weintraub‡ and Alexander Von Moll§
Air Force Research Laboratory, Wright-Patterson Air Force Base, Ohio, 45433

I. Introduction

In today's highly contested environment with near-peer adversaries, air supremacy is not a guarantee. These adversaries are likely to have extensive anti-aircraft defense systems and pose a threat to aircraft attempting to provide close air support to mission troops [1]. The United States Air Force Science and Technology Strategy states its vision for 2030 and beyond to identify where adversaries cannot easily go, and ensure that the United Sates Air Force is capable of operating in that airspace [2]. In accordance with this vision, building the capability to passively navigate around adversarial IADS provides potential advantages in ensuring air superiority.

The work herein evaluates multiple Surface-to-Air-Missiles (SAMs). To approximate the range and lethality of the SAM, the air defense system is modeled as a cardioid. Many SAMs rely on the line of sight (LOS) angle to the aircraft [3]. Thus with proper maneuvering, aircraft can manipulate the threat region of the SAM to evade capture. The LOS angle of the SAM and the heading angle of the aircraft dictate the range and maneuverability of the SAM. In other words, the range of the WEZ is completely dependant on the state space of the aircraft. Thus the dynamic Weapon Engagement Zone (WEZ) in this paper is modeled as a cardioid, which is a function of the LOS angle of the SAM and the bearing angle of the aircraft. This WEZ rotates and changes size based on these angles to represent how a SAM contains only a specific amount of maneuverability and energy to engage an aircraft depending on that aircraft's orientation with respect to the SAM.

II. Background

There has already been considerable research done with trajectory planning optimization for obstacle avoidance using methods such as mixed-integer linear programming [4]. Multiple constraint problems have been analyzed with both two and three dimensions of freedom [5–8], each using minimal number of constraints to assure convergence. Dynamic constraints have been implemented with known [9, 10] or stochastic [11] trajectories, but do not depend on the aircraft's state space. Collision avoidance between two aircraft has been researched using stochastic estimation to give more realistic path planning where perfect knowledge of the adversary is not known [12]. Solving these optimal control problems yield path planning solutions which can provide tactical insight for pilots or can be implemented via navigational waypoints.

Research on surface to air missile avoidance has been shown for a scenario in three dimensions and the SAMs modeled as a cube [13]. In this work, the evading vehicle was constrained to maneuvers in either the horizontal or the vertical plane, while the SAM missile was free to maneuver in both planes. The optimal control problem in this work was to maximize the relative distance between the evader aircraft and the SAM missile at the time of closest approach. This optimal control problem was executed using different velocity ratios between the evader aircraft and the SAM, and different initial flight path and heading angles of the missile. The conclusion of the work is quite useful, in that horizontal maneuvers result in a larger miss distance with the missile than vertical maneuvers. In particular, the results illustrate the importants of the initial flight path angle of the missile. Depending on the missile's initial flight path angle, an inward or outward horizontal maneuver should be utilized to fly quickly over the missile's LOS. Because the SAM

*Graduate Student, Department of Aeronautics & Astronautics, Air Force Institute of Technology, 2950 Hobson Way, WPAFB, OH 45433.
†Assistant Professor, Department of Aeronautics & Astronautics, Air Force Institute of Technology, 2950 Hobson Way, WPAFB, OH 45433.
‡Electronics Engineer, Controls Science Center, Air Force Research Laboratory, WPAFB, OH 45433, AIAA Senior Member.
§Research Engineer, Controls Science Center, Air Force Research Laboratory, WPAFB, OH, 45433.

relies on its LOS angle to the target, being able to quickly change the LOS angle will make it more difficult for the SAM to react to the aircraft's evasive maneuver due to the SAM's LOS rotation rate limitation. Thus, when attempting to avoid a SAM, horizontal evasive maneuvers should be considered. This solution applies directly to the work herein and emphasizes the utility of solution in a two-dimensional plane.

An additional way to solve this optimal path problem is to use a constrained shortest path (CSP) model. In previous work, a CSP model was used to discretize the available airspace for an aircraft [14] [15]. This work considered multiple constraints to the airspace including surface to air missiles, turn radius limitations, terrain, etc. Modeling these constraints as polygonal shapes allowed for the airspace to be discretized into a grid, effectively eliminating constraints from the search space. Although this analysis was effective, only static constraints were considered.

To increase computational efficiency, the direct orthogonal collocation method [16] using GPOPS-II can be seeded with a non-optimal solution [17]. Humphrey's used direct orthogonal collocation in conjunction with PSM to avoid path constraints. His work implemented particle swarm optimization to find potential path solutions through multiple constraints modeled as superquadrics [18]. These path solutions were then used to seed the optimal control problem, greatly increasing convergence properties at the added expense of the pre-processing PSO operation. Dynamic threats modeled in the work were pre-defined and only traversed along road networks and were not influenced by the aircraft state trajectory.

Obstacle avoidance is by no-means a new problem. Two surveys cover obstacle avoidance and highlight a number of recent techniques for addressing this task in the presence of static and dynamic environments [19, 20]. The task we have in this paper addresses a unique dynamic obstacle that is dependent upon the vehicle states, and this coupling of vehicle strategy to the size and shape of the obstacle provides tactical and strategic insight for Air Force missions. The dynamics, control, and conditions for optimality are derived from previous work [21], and extended herein by adding the vehicle's heading as a state with control on the vehicle's heading rate. That work solved the optimal control problem by first examining the solution through indirect methods, then illustrating convergence of a solution with a single WEZ through even collocated direct methods. However, when using these methods, solution become intractable when increasing the fidelity of the dynamics model or including a second WEZ. This work implements direct orthogonal collocation methods to handle both of these cases.

III. Optimal Control Problem

In this optimal control problem, the aircraft (T), will reach a desired final location (F) in minimum time while completely avoiding the WEZ. The state vector is described as

$$\mathbf{x}(t) = [x_T(t), y_T(t), \psi(t)]^\top \in \mathbb{R}^3 \tag{1}$$

with the state dynamics and control described as functions of the aircraft's velocity,v_T, and heading angle ψ_T:

$$\mathbf{f}(t, \mathbf{x}(t), u(t); v_T) = \begin{bmatrix} \dot{x}_T(t) \\ \dot{y}_T(t) \\ \dot{\psi}(t) \end{bmatrix} = \begin{bmatrix} v_T \cos(\psi(t)) \\ v_T \sin(\psi(t)) \\ u(t) \end{bmatrix}. \tag{2}$$

The aircraft's velocity is assumed to be constant and equal to 1 in order to conform to a multitude of potential mission scenarios. The vehicle's control is on the aircraft's heading rate. In the first scenario, the initial and final state are set to validate the single WEZ solution found in previous work [21], but now using direct orthogonal collocation methods. The initial state is set with with a free initial heading at $\mathbf{x}_0 = \mathbf{x}(t_0) = [1, 3, \text{free}]^\top$, and must end at a desired final location with a free final heading, $\mathbf{x}_F = \mathbf{x}(t_f) = [-0.5, -3, \text{free}]^\top$. The bounds on the state and control were chosen to define the domain and provide tractable solutions. These bounds are listed below:

$$\begin{aligned} |x_T(t)| &\leq 20, \forall\, t \in [0, t_f] \\ |y_T(t)| &\leq 20, \forall\, t \in [0, t_f] \\ |\psi(t)| &\leq \pi, \forall\, t \in [0, t_f] \\ |u(t)| &\leq 0.78(\text{rad/s}), \forall\, t \in [0, t_f]. \end{aligned} \tag{3}$$

The WEZ is implemented as a dynamic path constraint for the aircraft and is derived as a function of four parameters. These include the line of sight angle from the WEZ origin to the target, $\lambda \in [0, 2\pi)$, the pointing angle of the WEZ defined as the angle from the origin to any arbitrary point in state space, $\theta \in [0, 2\pi)$, the relative bearing angle from the

aircraft to the WEZ origin, $\zeta \in [0, 2\pi)$, and of the maximum possible range of the WEZ, R_{max}. The WEZ is defined as the general cardioid function, given below in polar coordinates

$$\rho(\theta, \lambda, \zeta) = \frac{R_{max}}{2} \frac{\cos\zeta + 1}{2} (1 + \sin(\pi/2 - \lambda + \theta)). \tag{4}$$

The worst case scenario for the aircraft occurs when the WEZ is oriented directly at the aircraft, giving the WEZ its maximum range when $\theta = \lambda$. Simplifying the general cardioid equation for this worst case scenario results in the maximum range of the cardioid at a certain instance in time as

$$\rho_{max}(\zeta) = \frac{R_{max}}{2} (\cos\zeta + 1). \tag{5}$$

It is important to note that ρ_{max} is only equal to R_{max} if the heading angle of the aircraft is pointed directly at the WEZ origin. Otherwise, ρ_{max} is always smaller than R_{max}, as the missile from the SAM will have to expend additional energy to reach the aircraft. To create the dynamic cardioid using Cartesian coordinates, the following equations were used:

$$\begin{aligned} \lambda(\mathbf{x}(t)) &= \tan^{-1}\left(\frac{y_T}{x_T}\right), \\ AA(\mathbf{x}(t)) &= -\pi - \lambda(\mathbf{x}(t)), \\ \zeta(\mathbf{x}(t), \psi(t)) &= \psi(t) + AA(\mathbf{x}(t)), \end{aligned} \tag{6}$$

This results in the x and y Cartesian coordinates, x_{wez} and y_{wez},

$$\begin{aligned} x_{wez} &= \rho(\theta, \lambda, \zeta)\cos\theta, \\ y_{wez} &= \rho(\theta, \lambda, \zeta)\sin\theta. \end{aligned} \tag{7}$$

Finally, the distance from the origin of the WEZ to the aircraft is defined as

$$d(t) = \sqrt{x_T^2(t) + y_T^2(t)}. \tag{8}$$

The figure below maps the scenario for this optimal control problem, with the airplane depicting the aircraft, and the blue cardioid emanating from the origin as the WEZ.

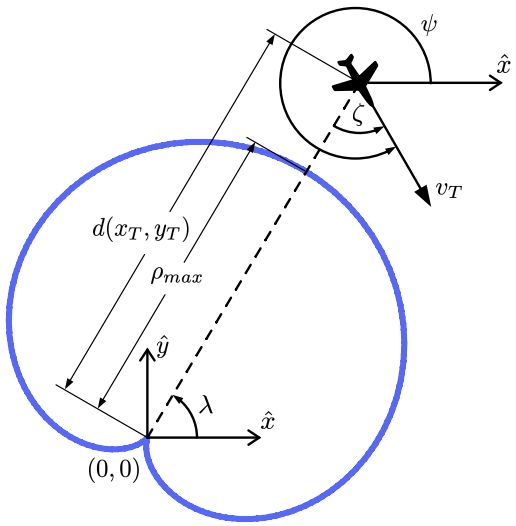

Fig. 1 Schematic of the Weapon Engagement Zone Avoidance Scenario

With the scenario defined, the optimal control problem can now be posed. The goal is to reach the desired end location in minimum time while avoiding the WEZ, which yields the value function of the optimal control problem:

$$V(\mathbf{x}) = \underset{u(t)}{\operatorname{argmin}}\, J = \underset{u(t)}{\operatorname{argmin}} \int_0^{t_f} \mathrm{d}t \tag{9}$$

subject to the dynamics defined in (2) and the inequality path constraint:

$$g(\mathbf{x}) = \rho_{max}(\zeta) - d(x_T, y_T) \leq 0 \; \forall \; t \in [0, t_f]. \tag{10}$$

Previous work has shown the solution to this problem with a singular WEZ using direct even collocated methods for optimal control [21]. From this, the previous work found that the optimal strategy for the aircraft to reach the desired end point is to be on a straight-line trajectory when the aircraft is not on the boundary of the WEZ, and to travel along the boundary of the WEZ when the WEZ inhibits a straight-line path to the desired end point. Solving optimal control problems using indirect methods can provide an analytical solution, but some problems simply become intractable due to their complexity and number of variables. Because of this, a direct orthogonal collocation method approach is used for a direct comparison and to investigate this optimal control problem with more complexity.

IV. Simulation

A. Single WEZ Solution

The solution from GPOPS-II was obtained by seeding the algorithm with an initial guess of $[x_0, x_F]$, and an R_{max} of the WEZ set to 2 distance units (DU). The solution in GPOPS-II was very rapid, with a solution converging in 1.96 seconds, on a computer with 16 GB of RAM and an Intel® Core™ i7-6500U CPU processor.

To visualize the dynamic nature of the WEZ, Figure 2 demonstrates how the WEZ will change its size and orientation according to the aircraft's relative position. The lines of the WEZ become darker as time increases to depict the dynamic nature of the WEZ. The aircraft begins at the point [1,3]. It starts on a straight-line path offset from the end point of

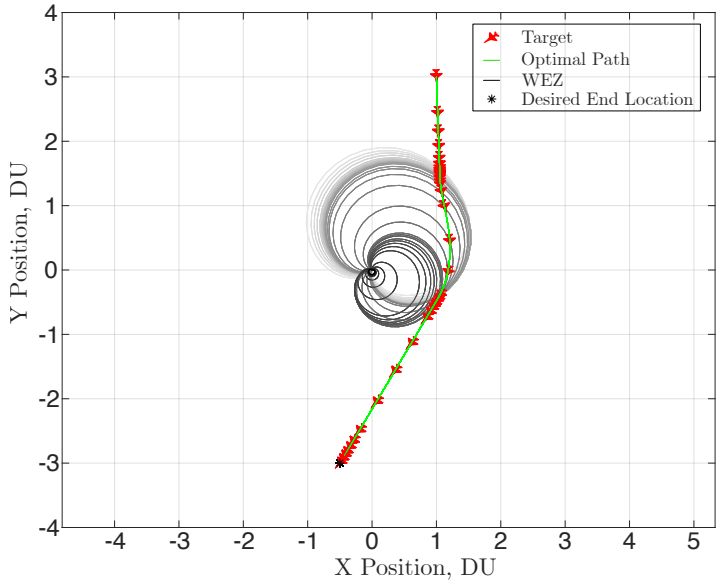

Fig. 2 Time History of the Optimal Control Solution

[-0.5,-3]. Once the vehicle has a straight-line path at the desired end point, it leaves the tangential path along the WEZ, and heads straight for the end location. The WEZ range is large when the aircraft is straight out in front of it, but as the aircraft begins to move around the WEZ, its range begins to decrease because the LOS angle begins to decrease, representing the increased energy required for the SAM to hit the aircraft. The aircraft reached the desired end location in 6.5 seconds.

One of the advantages to using GPOPS-II is that the value of the costates can be gathered from the solution. With insight into the value of the costates, the value of the Hamiltonian along the trajectory can be found. In general, the Hamiltonian is defined as the Lagrangian plus the costates, $\boldsymbol{\lambda}$, multiplied by the state dynamics.

$$\mathcal{H} = \mathcal{L} + \boldsymbol{\lambda} \cdot \mathbf{x} \tag{11}$$

Since this optimal control problem is for minimum time, there is no value for the Lagrangian, and the Hamiltonian is just the costates multiplied by the dynamics:

$$\mathcal{H} = \lambda_x v_T \cos(\psi(t)) + \lambda_y v_T \sin(\psi(t)) + \lambda_\psi u(t) \tag{12}$$

These results confirm the solutions found in previous work [21]. First, the aircraft maintains a constant heading, transitioning to the edge of the constraint, followed by a constant heading to the target location. Second, by calculating the co-states from the optimal solution, the Hamiltonian was found to be constant over the trajectory with a value of -1, which is consistent with the tranversality conditions that exist, stating $\mathcal{H}(t_f) + 1 = 0$ [22].

Finally, Table 1 below compares the flight time of the even collocated solution [21] versus the direct orthogonal collocation solution under identical scenario parameters. Although the times are essentially equal, the direct orthogonal method shows a slight advantage in calculating the optimal solution. This time difference is due to the difference in location of the collocation points. Moreover, both the direct even collocated method and the direct orthogonal collocated method produced in GPOPS-II gave viable trajectories. The next scenarios evaluate complexities involving multiple constraints where analytical approaches quickly become intractable.

Table 1 Direct Methods Solution Time Comparison

Methodology	Flight Time
Even Collocation	6.472 sec
Direct Orthogonal Collocation	6.465 sec

B. Two WEZ Solution

An optimal control problem is introduced where there are two WEZs, and the optimal path for minimum time must be found. In this scenario, The initial and final conditions define the aircraft position and heading angle. The start location of the aircraft is [10,0, $-\pi/2$], and the desired end location is [-4,0,free]. Both of the WEZs have an R_{max} of 4, and the center of these WEZs are chosen to give the aircraft different approach scenarios. To illustrate this work, the emanating point of each cardioid must be known, since they are not at the origin, as seen in the single WEZ case. The coordinates for the center emanating point of the first cardioid are denoted as $[x_{c1}, y_{c1}]$, and the center emanating point for the second cardioid are denoted as $[x_{c2}, y_{c2}]$. To produce these cardioids in Matlab, two bearing angles and LOS angles exist, one for each cardioid, and these angles include the coordinates of the emanating points for each of the cardioids:

$$\begin{aligned} \lambda_1(x(t)) &= \tan^{-1}\left(\frac{y_T - y_{c1}}{x_T - x_{c1}}\right), \\ \lambda_2(x(t)) &= \tan^{-1}\left(\frac{y_T - y_{c2}}{x_T - x_{c2}}\right). \end{aligned} \tag{13}$$

These new LOS angles will update the remaining variables in Equation 6. The only other necessary change is to adjust the Cartesian coordinates of each cardioid to now include the coordinates of each respective emanating point. For cardioid 1:

$$\begin{aligned} x_{1,wez} &= \left(\frac{R_{max}}{2}\frac{\cos(\psi - \lambda_1 - \pi) + 1}{2}(1 + \sin(\pi/2 - \lambda_1 + \theta))\right)\cos\theta + x_{c1}, \\ y_{1,wez} &= \left(\frac{R_{max}}{2}\frac{\cos(\psi - \lambda_1 - \pi) + 1}{2}(1 + \sin(\pi/2 - \lambda_1 + \theta))\right)\sin\theta + y_{c1}, \end{aligned} \tag{14}$$

and for cardioid 2:

$$\begin{aligned} x_{2,wez} &= \left(\frac{R_{max}}{2}\frac{\cos(\psi - \lambda_2 - \pi) + 1}{2}(1 + \sin(\pi/2 - \lambda_2 + \theta))\right)\cos\theta + x_{c2}, \\ y_{2,wez} &= \left(\frac{R_{max}}{2}\frac{\cos(\psi - \lambda_2 - \pi) + 1}{2}(1 + \sin(\pi/2 - \lambda_2 + \theta))\right)\sin\theta + y_{c2}. \end{aligned} \tag{15}$$

With the two different cardioids now defined off the origin, the optimal control problem can be executed. This two WEZ scenario is varied with how far apart the two WEZ emanating points are from each other, called the Cardioid Separation Distance (CSD). The cardioid on the left will be referred to as Cardioid 1 and will have an initial emanating point of [-2.6,0]. The cardioid on the right in the scenario will be referred to as Cardioid 2, and its initial emanating point coordinates will start at [2.6,0]. The CSD will be decreased in subsequant simulations by moving both cardiods towards the origin.

1. Scenario 1: CSD Equates to ≤ 70% Overlap of R_{max}

The first orientation for the two WEZ scenario is for a CSD value that results in a WEZ overlap less than 70% of the R_{max} value. At the upper limit, this results with the emanating points for Cardioids 1 and 2 at $[\pm 2.6, 0]$ respectively. The time history of the optimal path is shown in Figure 3, with the darker lines indicating the range of the WEZ as time increases.

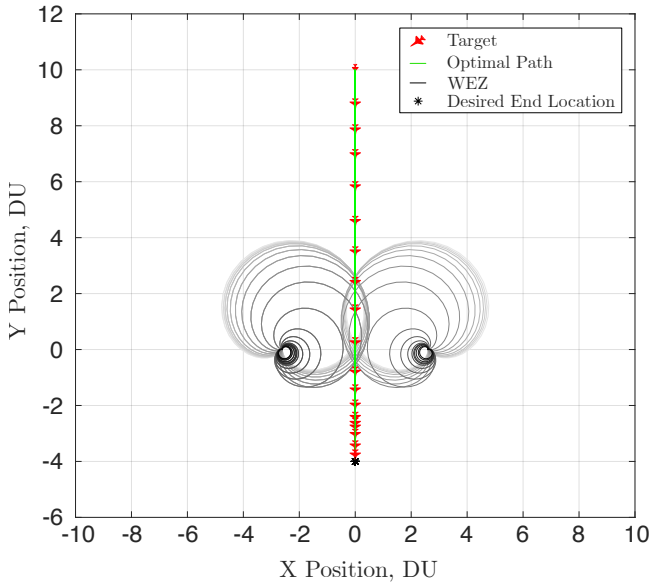

Fig. 3 Time History of the Optimal Path Solution with a CSD Greater than R_{max}

When the CSD equates to a value less than or equal to a 70% overlap of R_{max}, the WEZs do not overlap in a way that inhibits the aircraft from taking on a straight-line path to the end point. In the beginning of the scenario, the WEZs do overlap due to the larger LOS angle to the aircraft, but as the aircraft approaches the desired end location, the LOS angles for both WEZs decrease enough to where they no longer overlap, thus allowing the aircraft to take a straight-line path to the desired end location without violating a constraint. The aircraft reaches the desired endpoint in 14 seconds.

2. Scenario 2: CSD Equates to ≥ 75% Overlap of R_{max}

The second orientation for the two WEZ scenario is for a CSD value that results in a WEZ overlap greater than 75%. Cardioid 1 and Cardioid 2 have moved to the point $[\pm 2.5, 0]$ respectively. The time history of the optimal path is shown in Figure 4. Because of the exceedingly large overlap between the two WEZs, there is no feasible path for the aircraft to take that allows for it to go between the WEZs. Because of this, the aircraft must take a path around the WEZs in order to not violate a constraint. To get around the WEZs, the aircraft starts on a straight path to the right edge of Cardioid 2. Once it reaches the edge of this cardioid, it follows along it tangentially until a straight line path to the desired end point can be taken, consistent with the approach from the single WEZ scenario. The aircraft reaches the desired endpoint in 17.69 seconds, which is the slowest of all scenarios.

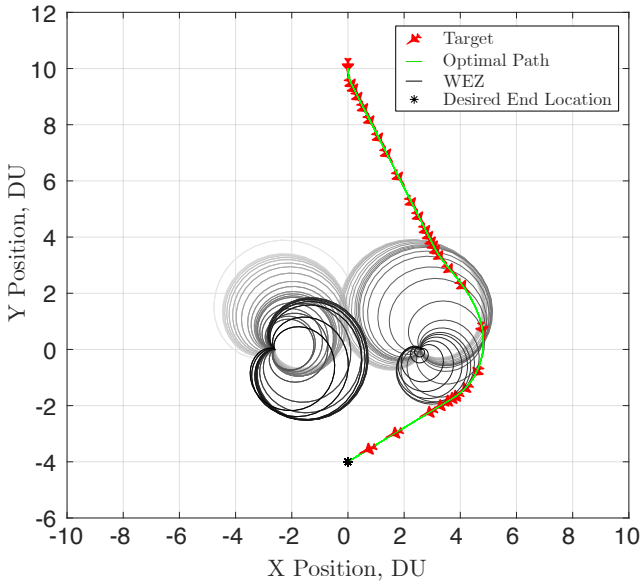

Fig. 4 Time History of the Optimal Path Solution with a CSD Smaller than R_{max}

3. Scenario 3: Interim Solution

The final orientation for the two WEZ scenario is for a CSD value that equates to a WEZ overlap that is greater than 70% but less than 75% of R_{max}. For this scenario, the position for Cardioid 1 and Cardioid 2 were chosen to be $[\pm 2.56, 0]$ respectively. Determining this range was accomplished through experimental perturbations of the CSD as analytical solutions for this problem are unlikely. The time history of this optimal path is shown in Figure 5. The aircraft

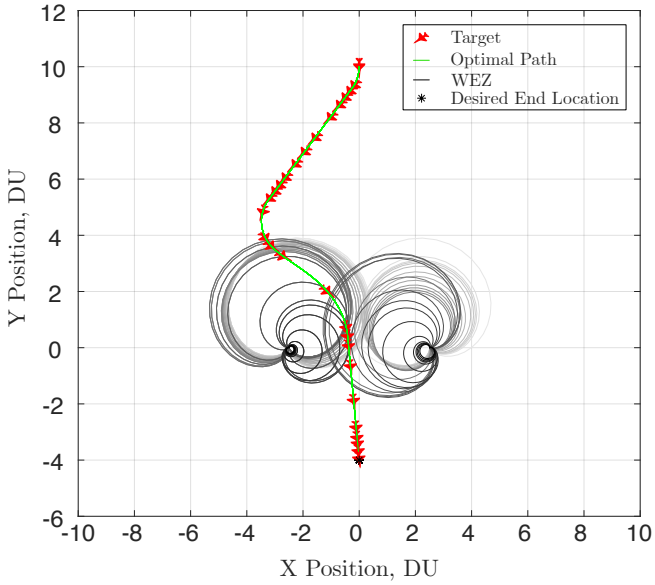

Fig. 5 Time History of the Optimal Path Solution with a CSD Equal to R_{max}

begins on a straight path headed out in front of Cardioid 1. As the aircraft is directly above Cardioid 1, it begins to turn and follow tangentially along Cardioid 1 towards the desired end location. With this maneuver, the aircraft uses its bearing angle to reduce the range of Cardioid 1. With the range of Cardioid 1 reduced, there now exists enough space between the two cardioids for the aircraft to go between them without violating either constraint. Figure 6 depicts the range of each WEZ, the bearing angle of the aircraft to each WEZ, and the LOS angle of each WEZ for this path

solution. The bold lines on each plot represent when the aircraft is tangent to each respective WEZ. It can be seen that in the beginning of the flight path as the aircraft travels towards Cardioid 1, its range increases. The aircraft then follows along the outer edge of Cardioid 1, illustrated by the bold red line, making its bearing angle close to 90 degrees and thus quickly decreasing the range of Cardioid 1. At around 13.5 seconds, at the end of the bold red line, it can be seen that the range of Cardioid 1 is slightly less than 3.2, which thus allows the aircraft to begin to split in between the WEZs. Once the aircraft gets in between the WEZs, the LOS and bearing angles quickly diverge as seen around 14 seconds in Figure 6, thus driving the ranges of the WEZs to zero and allowing for the aircraft to reach the desired end location. The aircraft reaches the desired endpoint in 16.34 seconds.

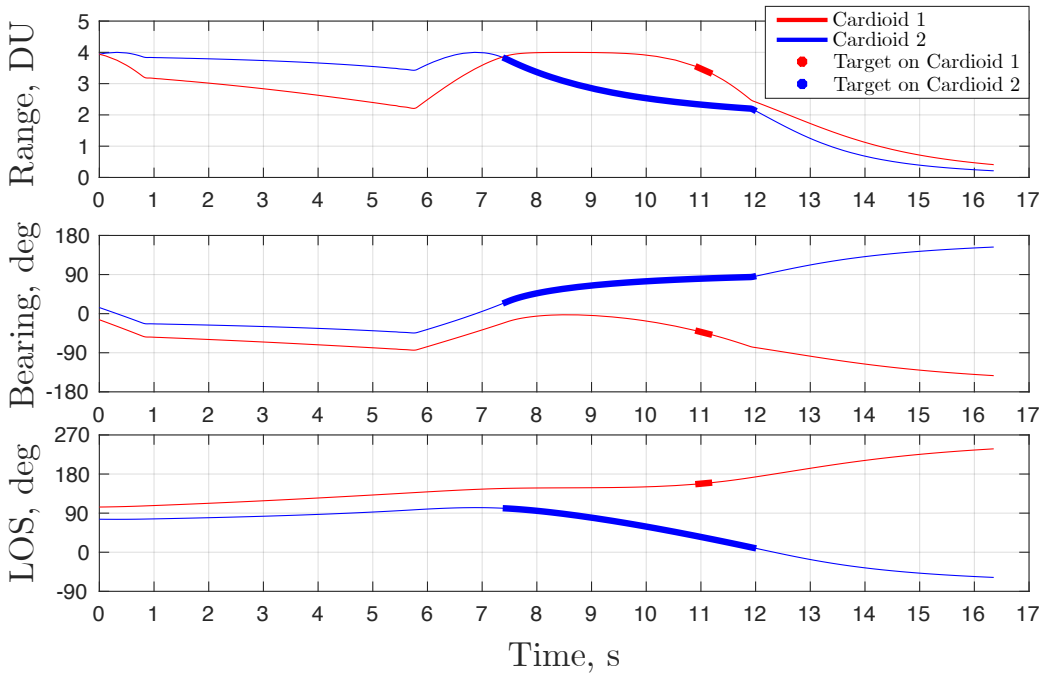

Fig. 6 WEZ Range Throughout Optimal Flight Path with CSD Equal to R_{max}

If the aircraft were to attempt to go on a straight line path for the end location through the cardioids without doing the beginning maneuver, the LOS angle of the WEZs and the bearing angle of the aircraft would both be 45 degrees at the same time, achieving an overlap of their threat regions, completely blocking a path through the cardioids.

V. Conclusions

This work extends previous work for aircraft WEZ avoidance by increasing the fidelity of the dynamics model, placing control on the vehicles heading rate, and by implementing direct orthogonal control methods to acquire converged solutions with multiple dynamic constraints. From the different multiple WEZ scenarios implemented, a strategy can be deduced. First, even though multiple WEZs can be constructed such that their threat regions overlap, there still exist a safe path solution through the environment. Given the parameters defined herein, a safe trajectory through two WEZs can be achieved up to a 75% overlap of the R_{max} value. Further, a straight line trajectory is optimal up to a 70% overlap of the R_{max} value. Of significant contribution is the region between these two thresholds upon which the aircraft can manipulate the LOS angle between the WEZ and the aircraft as well as the heading angle of the aircraft to build a trajectory to safely transit through the two WEZs without violating a constraint region. This is accomplished by first maneuvering in front of one of the WEZs, and by following it tangentially, it can affect the engagement zone of both WEZs until a straight line path to the desired end location is achieved.

Further insight can be gained regarding constraint limitations of the aircraft. Previous work hypothesized the optimal trajectory would consist of two straight line segments and a curved segment. The curved segment would align with the outer limits of the dynamic WEZ and can be achieved without maximizing the heading rate control limits of the aircraft, as typically seen in bang bang control. This work proves that hypothesis, showing the limits of

the trajectory are based solely on the dynamics of the WEZ. Further, by implementing direct orthogonal collocation methods, constraint functions were dynamically incorporated into the domain, upon which the size and shape of the constraint were completely based on the state space of the aircraft. These trajectory solutions were determined with a constant velocity and constant altitude with perfect knowledge of the vehicles location. Future work will consider several advancements. First, implementing the WEZs as soft constraints will allow for insight into strategies when completely avoiding the WEZ is not feasible. Second, consideration will be given to an enemy airborne WEZ, translating under a known path in additional to the dynamics dependant on the aircraft's state space. And finally, trajectories will be analyzed given uncertainty in the aircraft's sensor measurements to fully evaluate the threat region. These simple strategies determined herein can be implemented into mission planning for operations where enemy anti-aircraft systems are prevalent.

VI. Acknowledgments

This work was partially funded through the Air Force Research Laboratory, Aerospace Systems Directorate, Power and Controls Division under research proposal number 2022-016. The authors at the Air Force Institute of Technology would like to thank the sponsor for providing the challenging concept, background information, and continual support. The work herein has been approved for public release with unlimited distribution.

References

[1] Rempfer, K., "Here's How Improving Enemy Anti-Aircraft Threats put Pilots and Crews at Risk," *Air Force Times*, 2019.

[2] The Chief of Staff of the Air Force, "Science and Technology Strategy, Strengthening USAF Sceience and Technology for 2030 and Beyond," Tech. rep., United States Air Force, 2019.

[3] Kopp, C., "Evading the Guided Missile," *Aerospace Publications, Canberra, ACT, Australia*, 2014.

[4] Richard, A., and How, J. P., "Aircraft Trajectory Planning With Collision Avoidance Using Mixed Integer Linear Programming," *American Control Conference*, IEEE, Anchorage, AK, 2002, pp. 1936–1941. https://doi.org/10.1109/acc.2002.1023918.

[5] Zollars, M. D., Cobb, R. G., and Grymin, D. J., "Optimal SUAS Path Planning in Three-Dimensional Constrained Environments," *Unmanned Systems*, Vol. 07, No. 2, 2019, pp. 105–118. https://doi.org/10.1142/S2301385019500031.

[6] Aggerwal, R., , and Kumar, M., "Chance-Constrained Approach to Optimal path Planning for Urban UAS," *AIAA Scitech Conference*, AIAA, Orlando, FL, 2020, pp. 1–12. https://doi.org/10.2514/6.2020-0857.

[7] Geyer, M., and Johnson, E., "An Integrated Top-Down Approach to 3D Obstacle Avoidance for Unmanned Aerial Vehicles," *AIAA Guidance, Navigation and Control Conference and Exhibit*, Hilton Head, South Carolina, 2007. https://doi.org/10.2514/6.2007-6825.

[8] Lin, C. E., and Shao, P.-C., "Failure Analysis for an Unmanned Aerial Vehicle Using Safe Path Planning," *Journal of Aerospace Information Systems*, Vol. 17, No. 7, 2020, pp. 358–369. https://doi.org/10.2514/1.I010795.

[9] Zhao, F., Yu, J., Hua, Y., Dong, X., Li, Q., and Ren, Z., "Decoupled SCP-based trajectory planning in the complex environment for multiple fixed-wing UAV systems," *International Conference on Unmanned Aircraft Systems (ICUAS)*, IEEE, Dubrovnik, Croatia, 2022, pp. 670–675. https://doi.org/10.1109/ICUAS54217.2022.9836077.

[10] Yang, J., Qu, Z., Wang, J., Conrad, K. L., and Hull, R. A., "Real-time Obstacles Avoidance for Vehicles in the Urban Grand Challenge," *Journal of Aerospace Computing, Information, and Communication*, Vol. 4, No. 12, 2007, pp. 1117–1133. https://doi.org/10.2514/1.32761.

[11] Aggerwal, R., Soderlund, A., Kumar, M., and Grymin, D. J., "Risk-Aware Path Planning for Unamnned Aerial Systems in a Spreading Wildfire," *Journal of Guidance, Control, and Dynamics*, Vol. 45, No. 9, 2022, pp. 1692–1708. https://doi.org/10.2514/1.G006365.

[12] Smith, N. E., Cobb, R. G., Pierce, S. J., and Raska, V. M., "Optimal Collision Avoidance Trajectories for Unmanned/Remotely Piloted Aircraft," *Guidance, Navigation, and Control (GNC) Conference*, AIAA, Boston, MA, 2013. https://doi.org/10.2514/6.2013-4619.

[13] Ong, S. Y., Pierson, B. L., and Lin, C.-F., "Optimal Evasive Aircraft Maneuvers Against a Surface-To-Air Missile," *Proceedings, The First IEEE Regional Conference on Aerospace Control Systems*, IEEE, Westlake Village, CA, 1993, pp. 475–482. https://doi.org/10.1109/AEROCS.1993.720980.

[14] Royset, J. O., Carlyle, M. W., and Wood, K. R., "Routing Military Aircraft With A Constrained Shortest-Path Algorithm," *Military Operations Research*, Vol. 14, No. 3, 2009, pp. 31 – 52.

[15] Zollars, M. D., Cobb, R. G., and Grymin, D. J., "Optimal Path Planning for SUAS Target Observation through Constrained Urban Environments using Simplex Methods," *American Control Conference (ACC)*, IEEE, Milwaukee, WI, 2018, pp. 5094–5099. https://doi.org/10.23919/ACC.2018.8430987.

[16] Eide, J. D., Hager, W. W., and Rao, A. V., "Modified Legendre-Gauss-Radau Collocation Method for Optimal Control Problems with Nonsmooth Solutions," *Journal of Optimization Theory and Applications*, Vol. 191, 2021, pp. 600—-633. https://doi.org/10.1007/s10957-021-01810-5.

[17] Patterson, M. A., and Rao, A. V., "GPOPS-II: A MATLAB Software for Solving Multiple-Phase Optimal Control Problems Using hp-Adaptive Gaussian Quadrature Collocation Methods and Sparse Nonlinear Programming," *ACM Transactions on Mathematical Software*, Vol. 41, No. 1, 2014, pp. 1–37. https://doi.org/10.1145/2558904.

[18] Humphreys, C. J., "Optimal Control of an Uninhabited Loyal Wingman," Phd dissertation, Air Force Institute of Technology, Wright-Patterson AFB, OH 45433, 484 2016.

[19] Shitsukane, A., Cheriuyot, W., Otieno, C., and Mgala, M., "A Survey on Obstacles Avoidance Mobile Robot in Static Unknown Environment," *International Journal of Computer (IJC)*, 2018.

[20] Pandey, A., Pandey, S., and Parhi, D., "Mobile robot navigation and obstacle avoidance techniques: A review," *Int Rob Auto J*, Vol. 2, No. 3, 2017, p. 00022.

[21] Weintraub, I. E., Von Moll, A., Carrizales, C., Hanlon, N., and Fuchs, Z., "An Optimal Engagement Zone Avoidance Scenario in 2-D," *SciTech Forum*, AIAA, San Diego, CA & Virtual, 2022. https://doi.org/10.2514/6.2022-1587.

[22] Kirk, D., *Optimal control theory; an introduction*, Prentice-Hall, Englewood Cliffs, N.J, 1970.